logarithmic potential (spheroidal)

$$\Phi_{\rm eff} = \tfrac{1}{2}v_0^2 \ln\left(R^2 + \frac{z^2}{q^2}\right) + \frac{L_z^2}{2R^2}, \qquad (3.70)$$

for a given Lz
a special orbit

guiding centre:
minimum in $\Phi_{\rm eff}$.

$\frac{\partial \Phi_{\rm eff}}{\partial R} = 0$

$\frac{\partial \Phi_{\rm eff}}{\partial z} = 0$

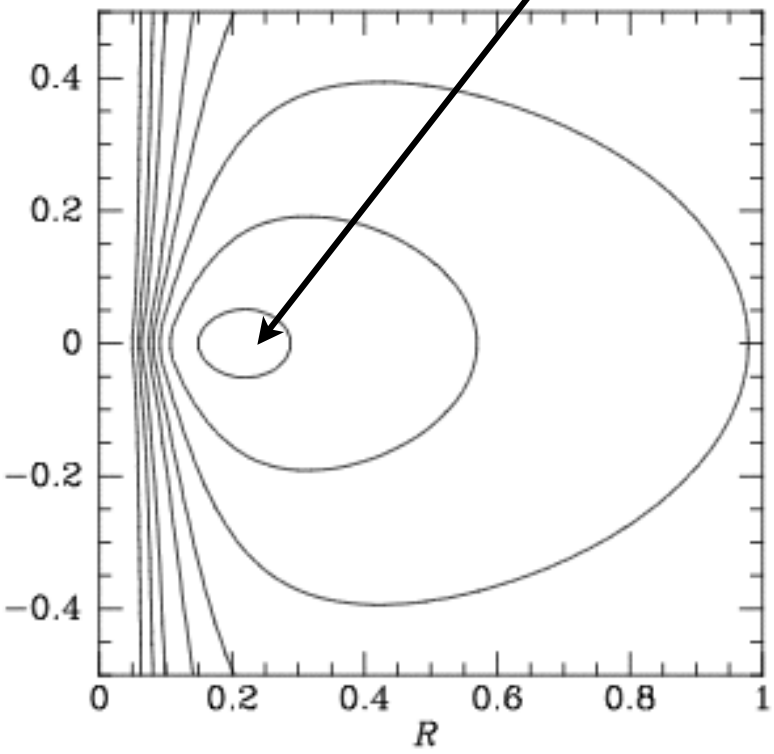

otential of equation (3.70) when $v_0 = 1$,
−0.5, 0, 0.5, 1, 1.5, 2, 3, 5. The axis ratio
ight.

different zvc for orbits of different E/Lz

The epicycle approximation

Epicycle direction are always retrograde;
opposite to planetary orbits

at apo-apse, moves slower relative to circular orbit

$$x(t) = X\cos(\kappa t + \alpha), \qquad y = -\gamma X \sin(\kappa t + \alpha) \equiv -Y\sin(\kappa t + \alpha).$$

$$\gamma \equiv \frac{2\Omega_g}{\kappa}$$

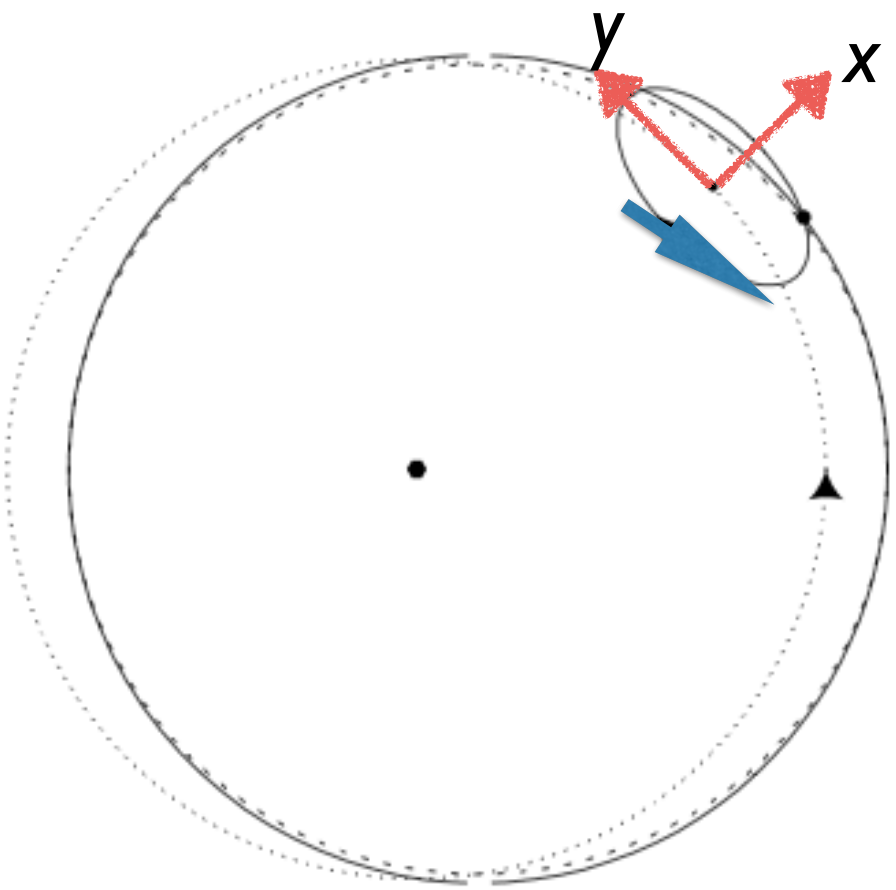

Keplerian: X/Y = 0.5
Harmonic: X/Y = 1
Galatic: X/Y ~ 0.7

$$\dot{x}^2 \equiv \sigma_R^2 = \tfrac{1}{2}\kappa^2 X^2$$
$$\dot{y}^2 \equiv \sigma_\theta^2 = \tfrac{1}{2}\kappa^2 Y^2$$

for stars with the same guiding center orbits

The epicycle approximation

vertical frequency: ν

radial frequency: κ

rotational frequency: Ω

independent measures of the potential

1st application: taking <v> of solar neighbourhood

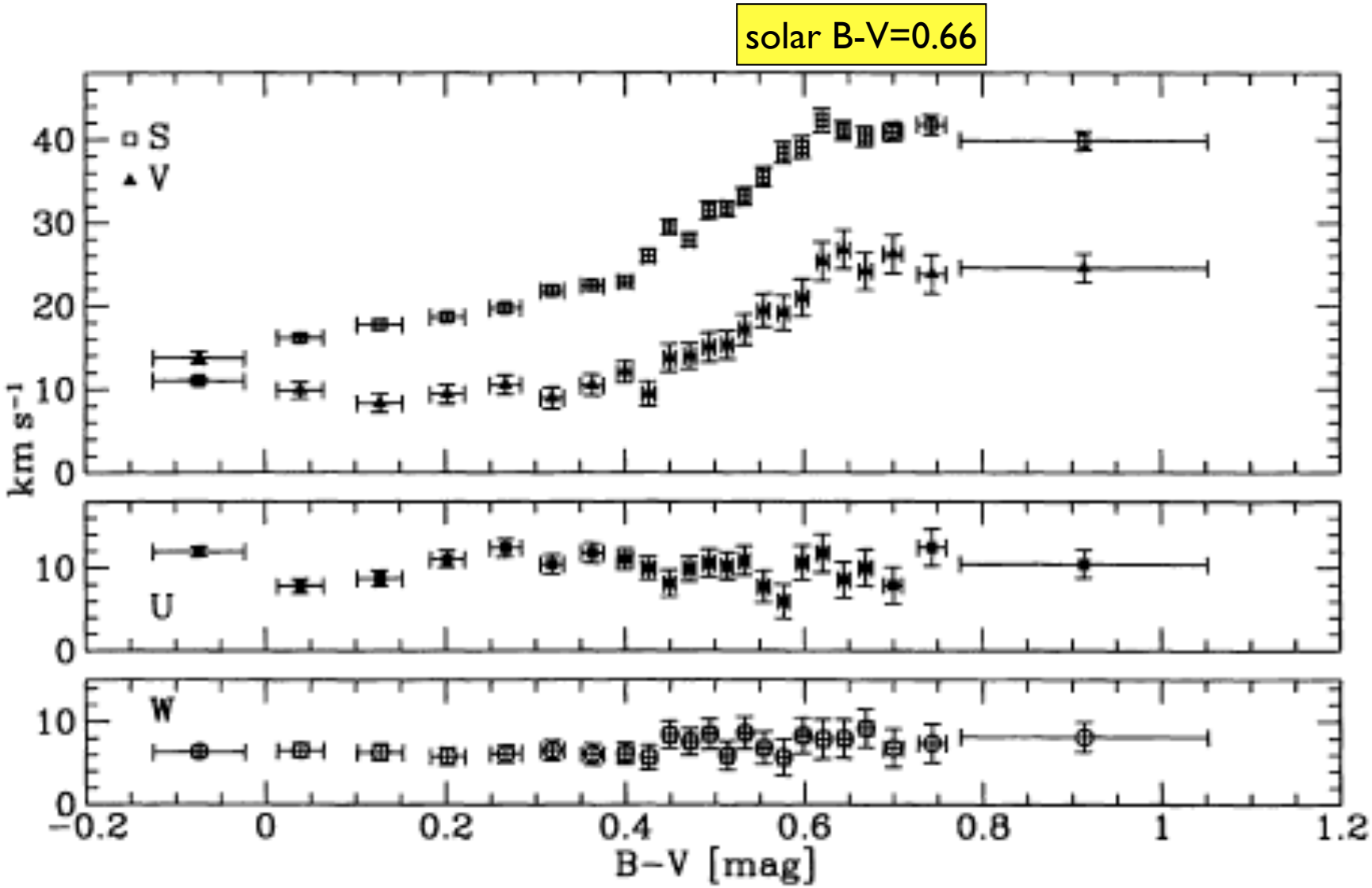

mponents U, V and W of the solar motion with respect to stars with different colour $B - V$. Also shown is the variation of the

2nd application: velocity dispersion

$$\sigma_i^2 = < (v_i - \bar{v}_i)^2 >$$

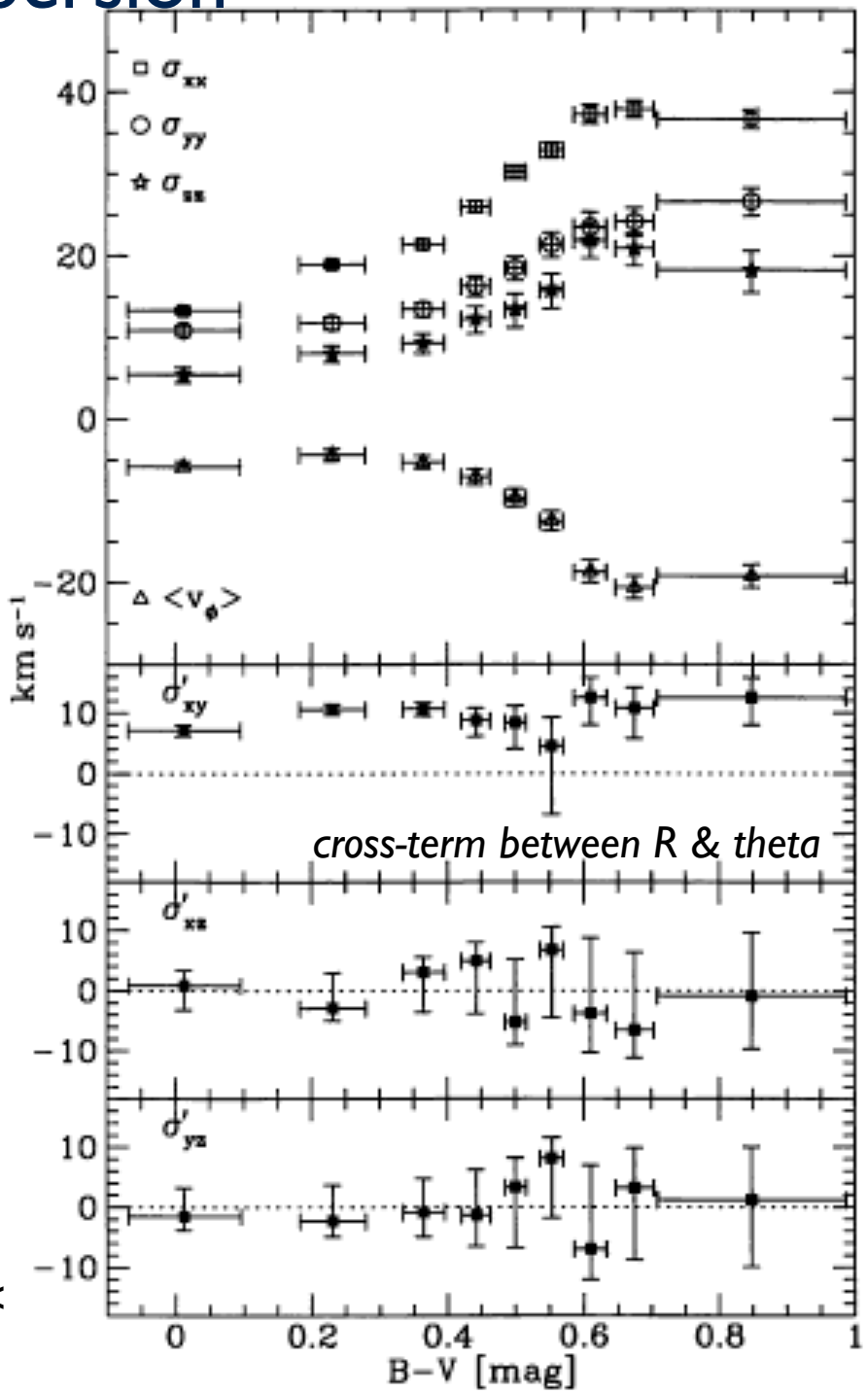

Figure 5. Velocity dispersions for stars in different colour bins. The top panel shows the mean rotation velocity (negative values imply lagging with respect to the LSR) and the three main velocity dispersions. In the three bottom panels $\sigma'_{ij} = \mathrm{sign}(\sigma^2_{ij})\,|\sigma^2_{ij}|^{1/2}$ is plotted for the mixed components of the tensor σ^2_{ij}.

for stars near the mid-plane (Hipparcos data, |z| < 100pc), Dehnen & Binney '98

Measuring Solar peculiar velocities (u_0, v_0, w_0)

by taking neighbourhood <V> averages

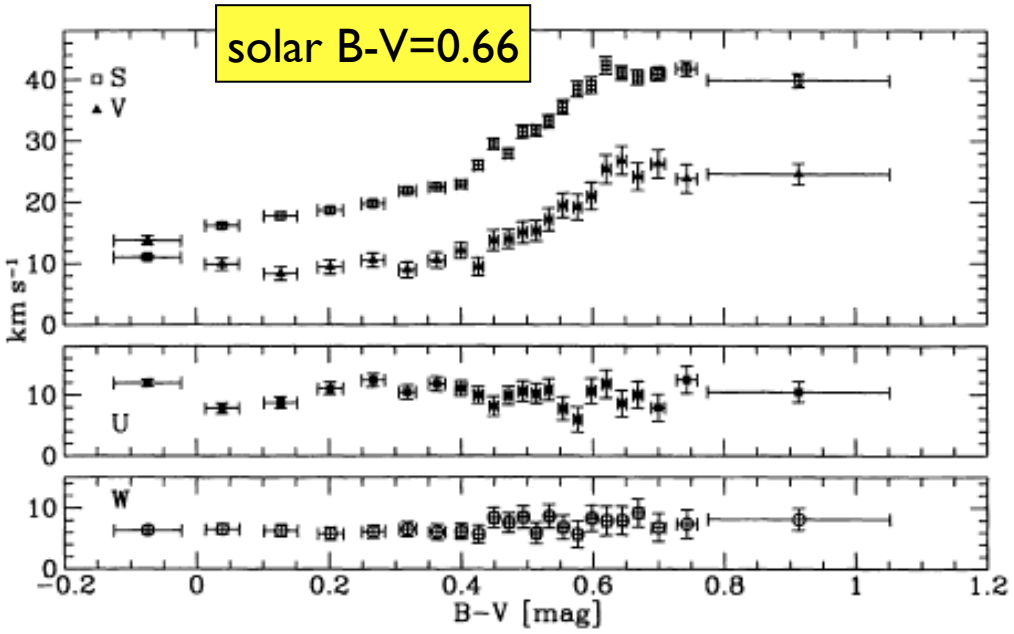

Figure 3. The components U, V and W of the solar motion with respect to stars with different colour $B-V$. Also shown is the variation of the dispersic colour.

extrapolating back to $S=0$. Ignoring stars blueward of $B-V=0$ mag we find

$$\begin{aligned} U_0 &= 10.00 \pm 0.36 \quad (\pm 0.08) \quad \mathrm{km\,s^{-1}}, \\ V_0 &= 5.25 \pm 0.62 \quad (\pm 0.03) \quad \mathrm{km\,s^{-1}}, \\ W_0 &= 7.17 \pm 0.38 \quad (\pm 0.09) \quad \mathrm{km\,s^{-1}}, \end{aligned} \tag{20}$$

Dehnen & Binney '98

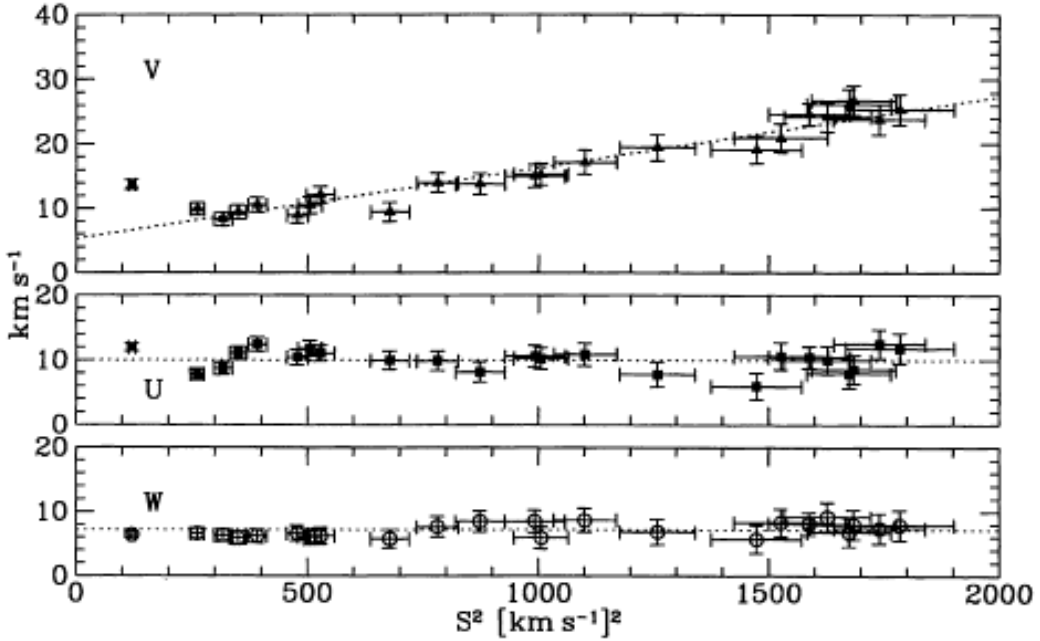

Figure 4. The dependence of U, V and W on S^2. The dotted lines correspond to the linear relation fitted (V) or the mean values (U and W) for stars b $B-V=0$.

Schematic distributions of local (u,v)

u: R-direction, x
v: theta-direction, y

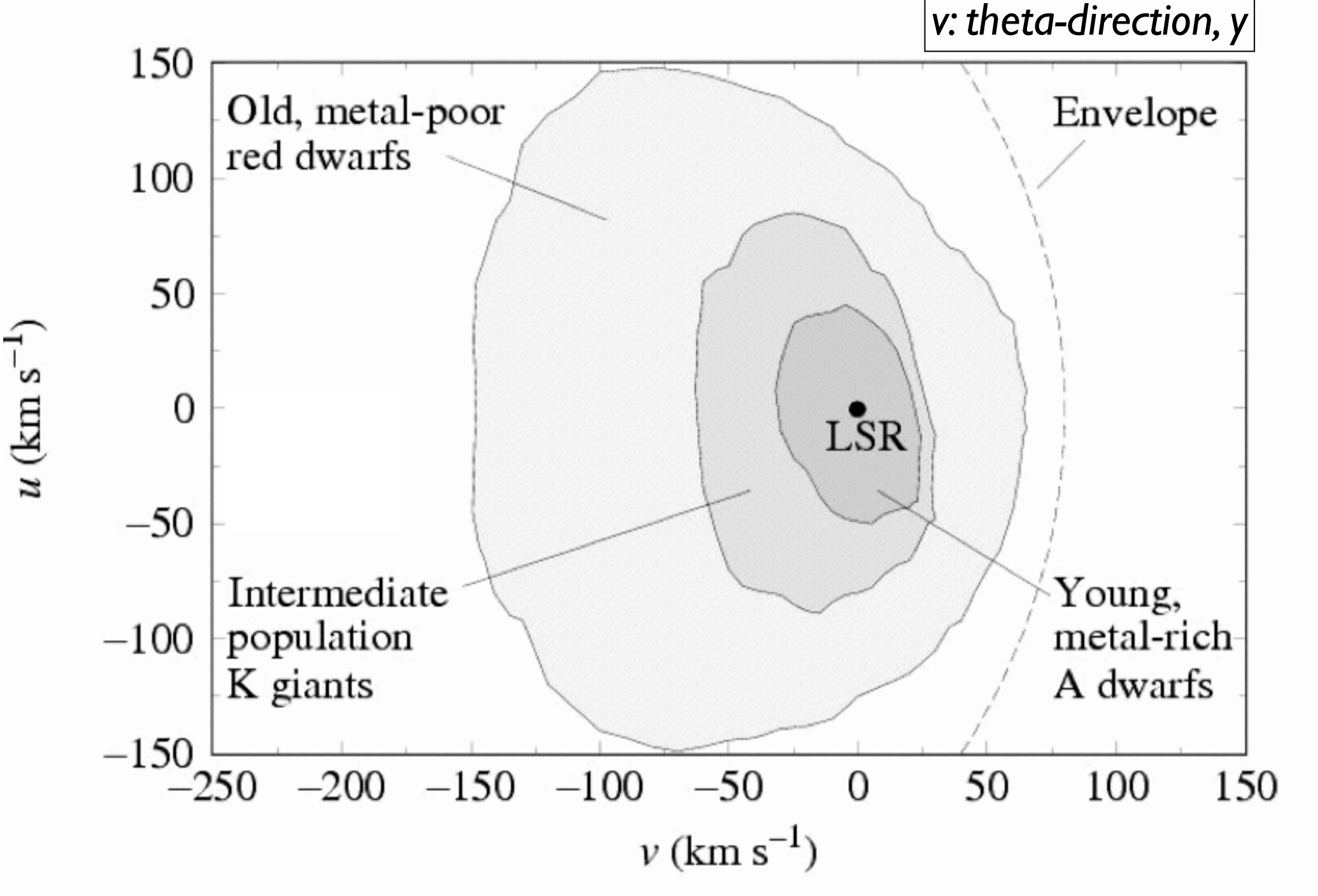

the ‘asymmetric drift’

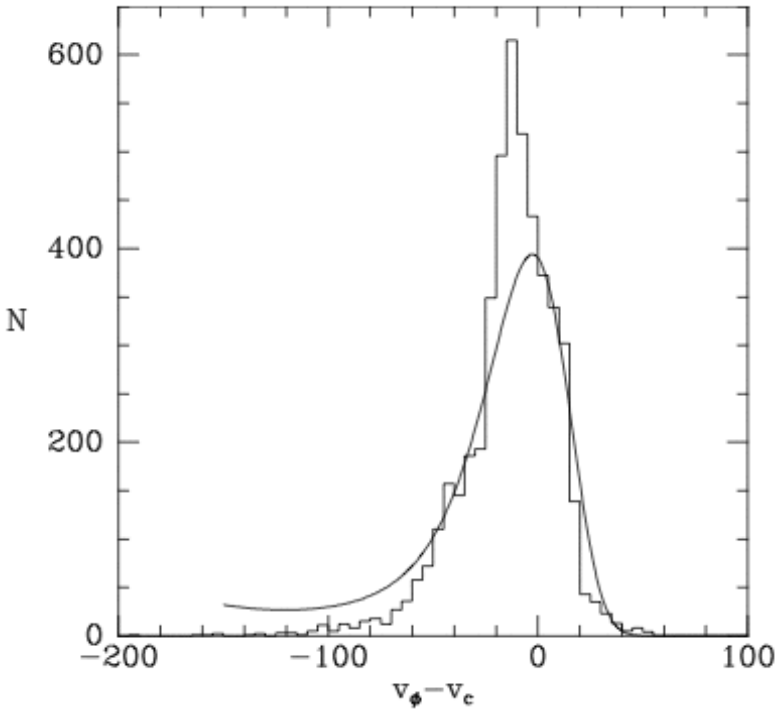

Figure 4.17 The distribution of v_ϕ components of 4787 F and G stars that have space velocities in Nordström et al. (2004). Stars with a high probability of having variable radial velocities are excluded. The smooth curve shows the distribution predicted by the Schwarzschild DF for a population with the same value of $\overline{v_R^2}^{1/2} = 34\,\mathrm{km\,s^{-1}}$.

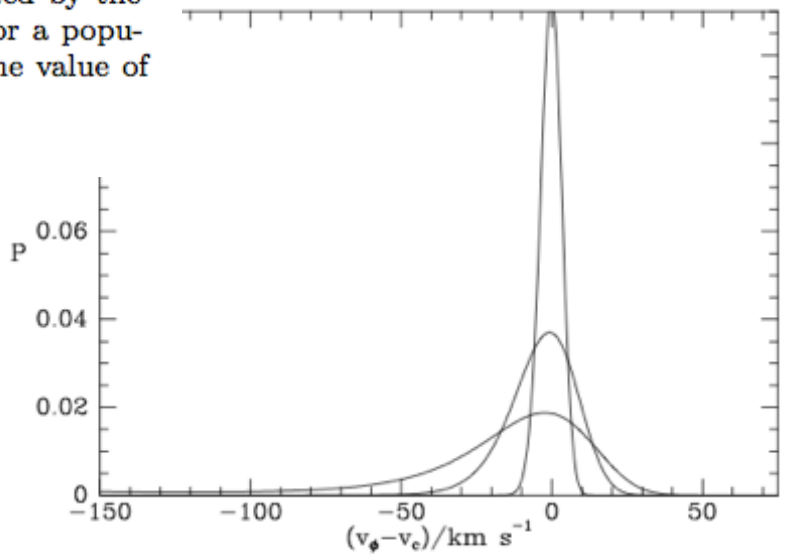

Figure 4.15 Three distributions of azimuthal velocities $\widetilde{v}_\phi$ predicted for stellar populations in the solar neighborhood by the DF (4.156). The circular speed has been assumed to be $v_0 = 220\,\mathrm{km\,s^{-1}}$ at all radii, $\sigma_R(L_z)$ and $\sigma_z(L_z)$ are taken to be proportional to $\exp[-L_z/(2v_0R_\mathrm{d})]$, while $\Sigma = \Sigma_0\exp(-R/R_\mathrm{d})$, with $R_0/R_\mathrm{d} = 3.2$ (Table 1.2). The values of $\overline{v_R^2}^{1/2}$ for the three populations are 5, 15 and $30\,\mathrm{km\,s^{-1}}$, the largest value producing the widest spread in $\widetilde{v}_\phi$.

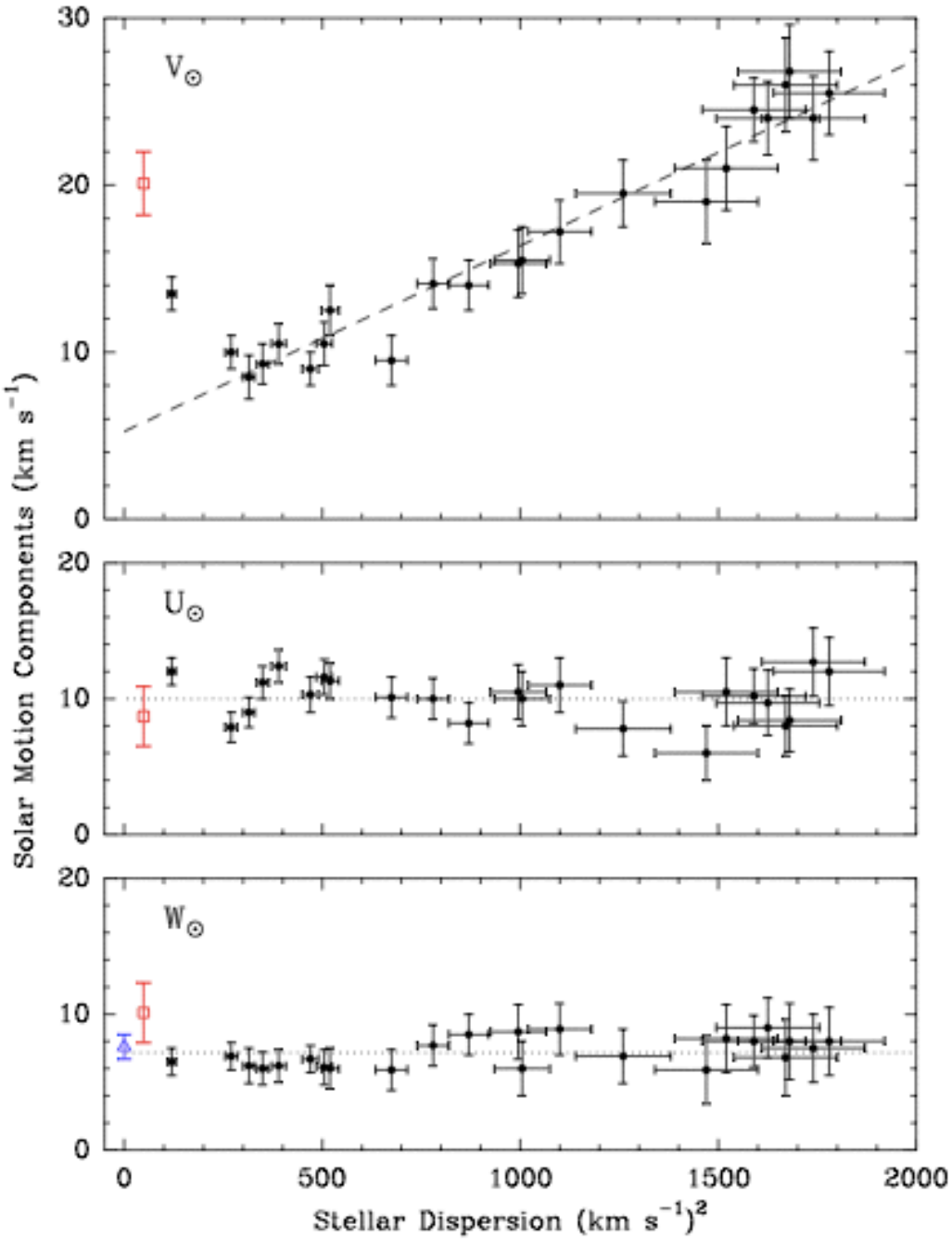

'asymmetric drift',
'rotational lag'
caused by two effects:
1)rotational support
2)density radial gradient

Reid et al '09: study of masers in star forming regions

Figure 4. Solar motion components determined from *Hipparcos* stars (i.e., the reflex of the average motion of stars) vs. stellar velocity dispersion after Dehnen & Binney (1998). Top Panel: $V_\odot$ is the Solar Motion in the direction of Galactic rotation (i.e., toward $\ell = 90°$). The "asymmetric drift" is shown with the dashed line. Middle Panel: $U_\odot$ is the Solar Motion toward the Galactic center. Bottom Panel: $W_\odot$ is toward the north Galactic pole. Also plotted at 50 (km s^{-1})^2 dispersion with open red squares are solar motion parameters obtained from the parallax and proper motions of star forming regions, and at zero dispersion with an open triangle is the $W_\odot$ component inferred from the proper motion of Sgr A* by Reid & Brunthaler (2004). Note the good agreement of the $U_\odot$ and $W_\odot$ components between *Hipparcos* and this study. The large deviation of the $V_\odot$ component from the asymmetric drift from this study is not indicative of large $V_\odot$ value, but points to a significant deviation from circular orbits for very young stars.

Different determinations of the solar peculiar motion

very young stars: dispersion reflects parent cloud orbit; moving groups...

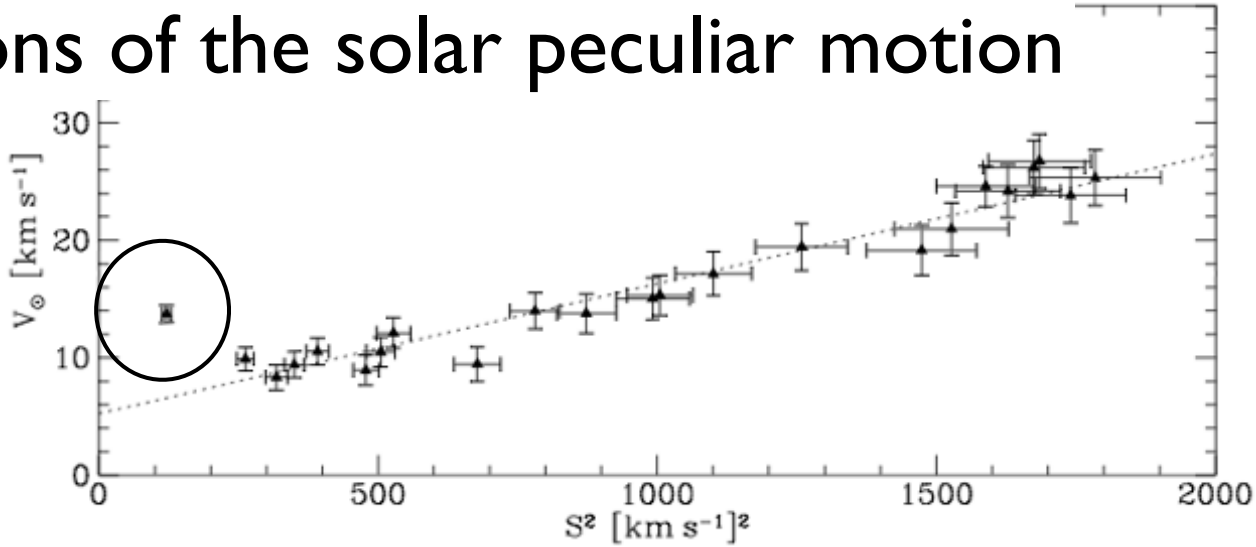

Figure 4.21 The asymmetric drift v_a for different stellar types is a linear function of the random velocity S^2 of each type. The vertical coordinate is actually $v_a + \tilde{v}_{\phi,\odot}$ where $\tilde{v}_{\phi,\odot}$ is the azimuthal velocity of the Sun relative to the LSR (after Dehnen & Binney 1998b).

Dehnen & Binney '98
(12,000 Hipparcos stars)

extrapolating back to $S = 0$. Ignoring stars blueward of $B - V = 0$ mag we find

$$U_0 = 10.00 \pm 0.36 \quad (\pm 0.08) \quad \mathrm{km\,s^{-1}},$$
$$V_0 = 5.25 \pm 0.62 \quad (\pm 0.03) \quad \mathrm{km\,s^{-1}}, \qquad (20)$$
$$W_0 = 7.17 \pm 0.38 \quad (\pm 0.09) \quad \mathrm{km\,s^{-1}},$$

Feast & Whitelock '97
(220 Cepheids)

$u_o = +9.3$ km s^{-1} (adc
tions);
$v_o = +11.2$ km s^{-1} (ad
tions);
$w_o = +7.61 \pm 0.64$ km s

Schonrich, Binney & Dehner '10
'the approach to the determination of V⊙ by DB98... is misleading'
(in fact, very young stars define V_0 perfectly)

U_0=11.1+/-0.7 km/s
V_0=12.2+/-0.5 km/s
w_0=7.3+/-0.4 km/s

Motion relative to the galactic centre can be measured.
= solar peculiar motion + rotation curve

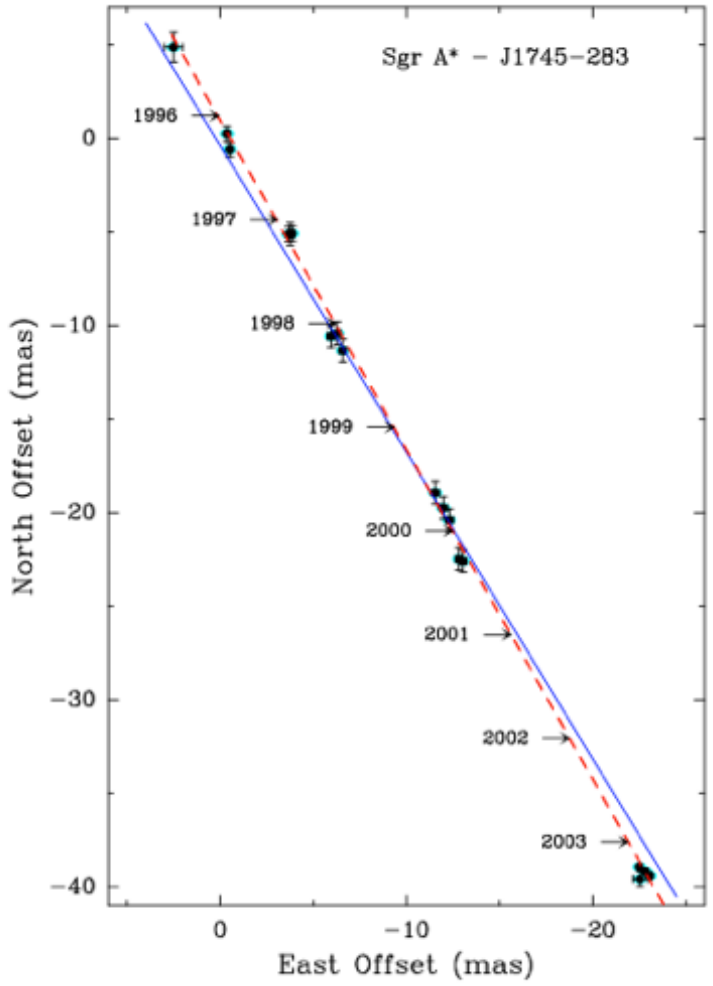

Fig. 1.— Position residuals of Sgr A* relative to J1745–283 on the plane of the sky. Each measurement is indicated with an ellipse, approximating the apparent scatter-broadened size of Sgr A* at 43 GHz and 1σ error bars, which include estimates of systematic uncertainties. The dashed line is the variance-weighted best-fit proper motion, and the solid line gives the orientation of the Galactic plane, which is tilted by 31.40° east of north in J2000 coordinates (see Appendix).

So rotation curve subject to bias in solar motion

More twists

Bovy et al '12, APOGEE data
v0 = 26 +/- 3 km/s; Milky Way mass down.

Table 2
Results for Galactic Parameters and Tracer Properties

Parameter	Flat Rotation Curve	Power-law $V_c(R) = V_c(R_0)\ (R/R_0)^{\beta}$
$V_c(R_0)$ (km s^{-1})	218 ± 6	218^{+4}_{-19}
β	...	$0.01^{+0.01}$
$dV_c/dR\,(R_0)$ (km s^{-1} kpc^{-1})	...	
A (km s^{-1} kpc^{-1})	$13.5^{+0.2}_{-1.7}$	
B (km s^{-1} kpc^{-1})	$-13.5^{+1.7}_{-0.2}$	
$(B^2 - A^2)/(2\pi G)$ ($M_\odot$ pc^{-3})	...	
Ω_0 (km s^{-1} kpc^{-1})	$27.0^{+0.3}_{-3.5}$	
R_0 (kpc)	$8.1^{+1.2}_{-0.1}$	
$V_{R,\odot}$ (km s^{-1})	$-10.5^{+0.5}_{-0.8}$	
$V_{\phi,\odot}$ (km s^{-1})	242^{+10}_{-3}	
$V_{\phi,\odot} - V_c$ (km s^{-1})	$23.9^{+5.1}_{-0.5}$	
$\mu_{\mathrm{Sgr\ A}^*}$ (mas yr^{-1})	$6.32^{+0.07}_{-0.70}$	$6.36^{+0.09}_{-0.86}$
$\sigma_R(R_0)$ (km s^{-1})	$31.4^{+0.1}_{-3.2}$	$32.2^{+0.2}_{-2.6}$
R_0/h_σ	$0.03^{+0.01}_{-0.27}$	$0.06^{+0.01}_{-0.17}$
$X^2 \equiv \sigma_\phi^2/\sigma_R^2$	$0.70^{+0.30}_{-0.01}$	$0.64^{+0.18}_{-0.02}$

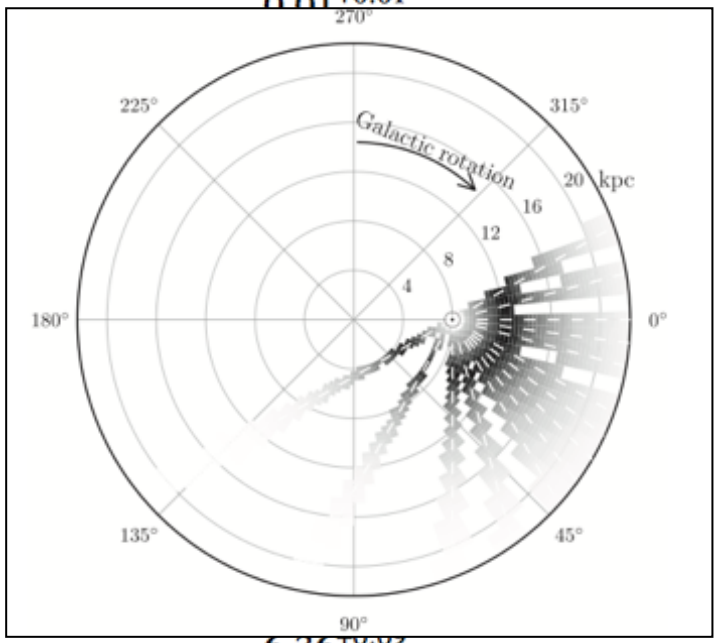

2nd application: velocity dispersion

$$\sigma_i^2 = < (v_i - \bar{v}_i)^2 >$$

velocity dispersion of stars increases with their mean ages

evidence for heating due to GMC or spiral arms/bars?

ratios of σ_R/σ_z, σ_R/σ_ϕ, cross-terms etc., constrain heating mechanisms

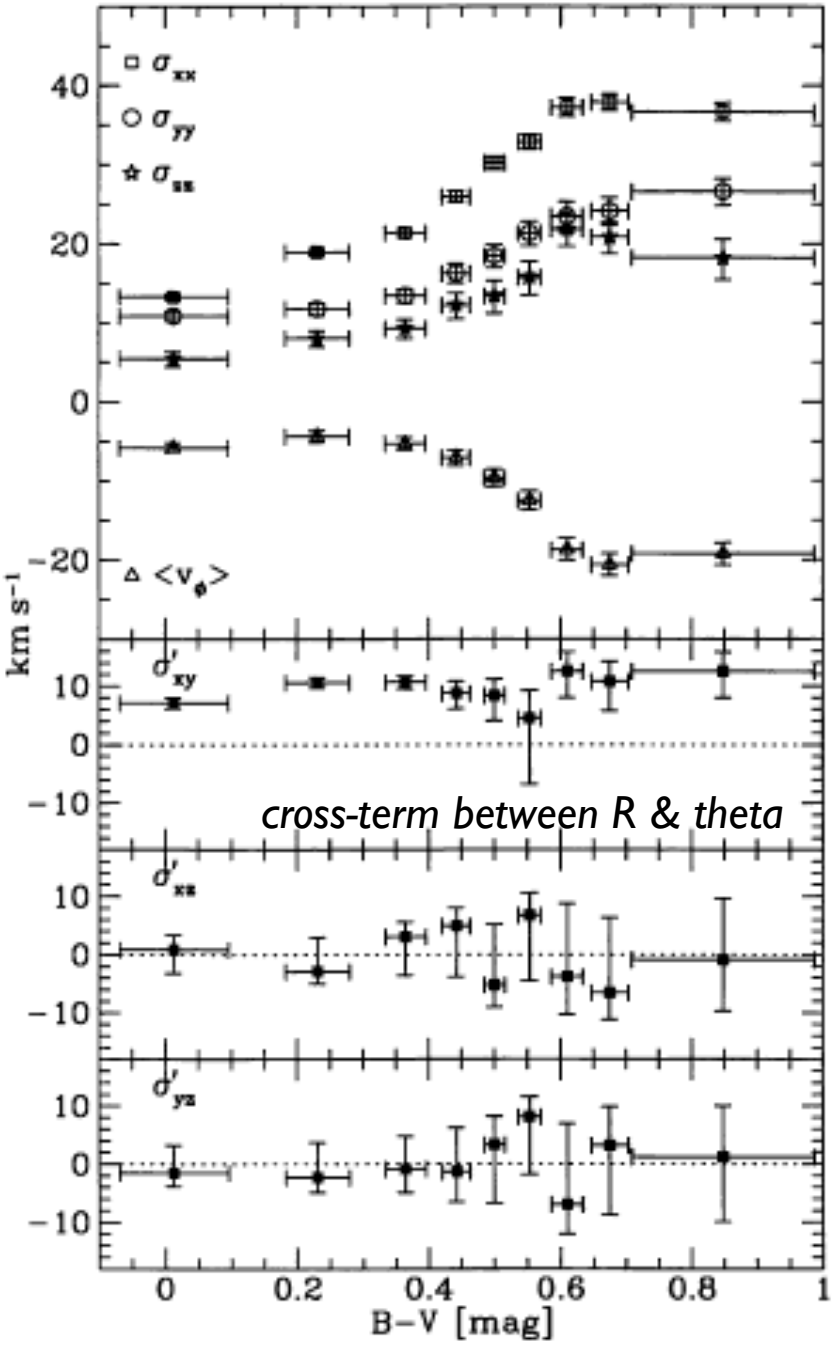

Figure 5. Velocity dispersions for stars in different colour bins. The top panel shows the mean rotation velocity (negative values imply lagging with respect to the LSR) and the three main velocity dispersions. In the three bottom panels $\sigma'_{ij} = \mathrm{sign}(\sigma^2_{ij})\,|\sigma^2_{ij}|^{1/2}$ is plotted for the mixed components of the tensor σ^2_{ij}.

for stars near the mid-plane (Hipparcos data, |z| < 100pc), Dehnen & Binney '98

ratio of σ_R/σ_ϕ also measures the gravitational potential

stars with the same guiding centres:

ratio of σ_R/σ_ϕ also measures the gravitational potential

$$x(t) = X\cos(\kappa t + \alpha), \qquad y = -\gamma X \sin(\kappa t + \alpha) \equiv -Y\sin(\kappa t + \alpha).$$

$$\gamma \equiv \frac{2\Omega_g}{\kappa}$$

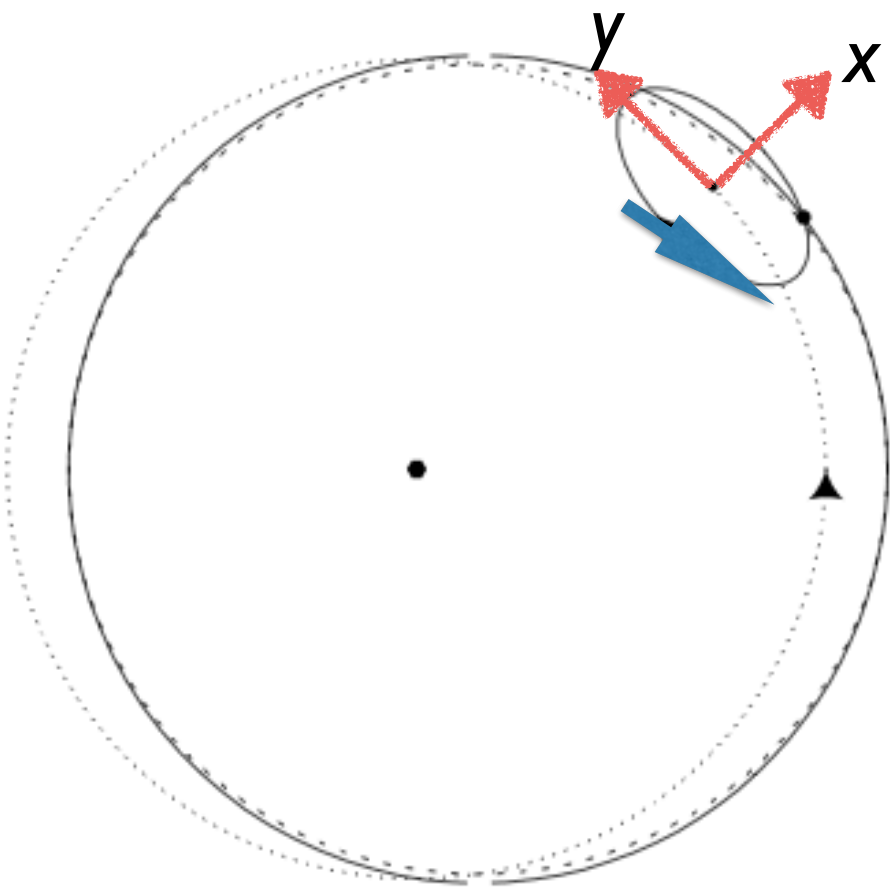

Keplerian: X/Y = 0.5
Harmonic: X/Y = 1
Galatic: X/Y ~ 0.7

$$\dot{x}^2 \equiv \sigma_R^2 = \tfrac{1}{2}\kappa^2 X^2$$
$$\dot{y}^2 \equiv \sigma_\theta^2 = \tfrac{1}{2}\kappa^2 Y^2$$

for stars with the same guiding center orbits

Practical problem: in the solar neighbourhood, stars have different guiding centres

Averaging over the phases α of stars near the Sun, we find

$$\overline{[v_\phi - v_c(R_0)]^2} = \frac{\kappa^2 X^2}{2\gamma^2} = 2B^2X^2. \qquad (3.98)$$

Similarly, we may neglect the dependence of κ on R_g to obtain with equation (3.84)

$$\overline{v_R^2} = \tfrac{1}{2}\kappa^2 X^2 = -2B(A-B)X^2. \qquad (3.99)$$

Taking the ratio of the last two equations we have

$$\frac{\overline{[v_\phi - v_c(R_0)]^2}}{\overline{v_R^2}} \simeq \frac{-B}{A-B} = -\frac{B}{\Omega_0} = \frac{\kappa_0^2}{4\Omega_0^2} = \gamma^{-2} \simeq 0.46. \qquad (3.100)$$

But stars also have different amplitudes (X is not a constant)

a distribution of X; centroid and dispersion depends on stellar ages; however…

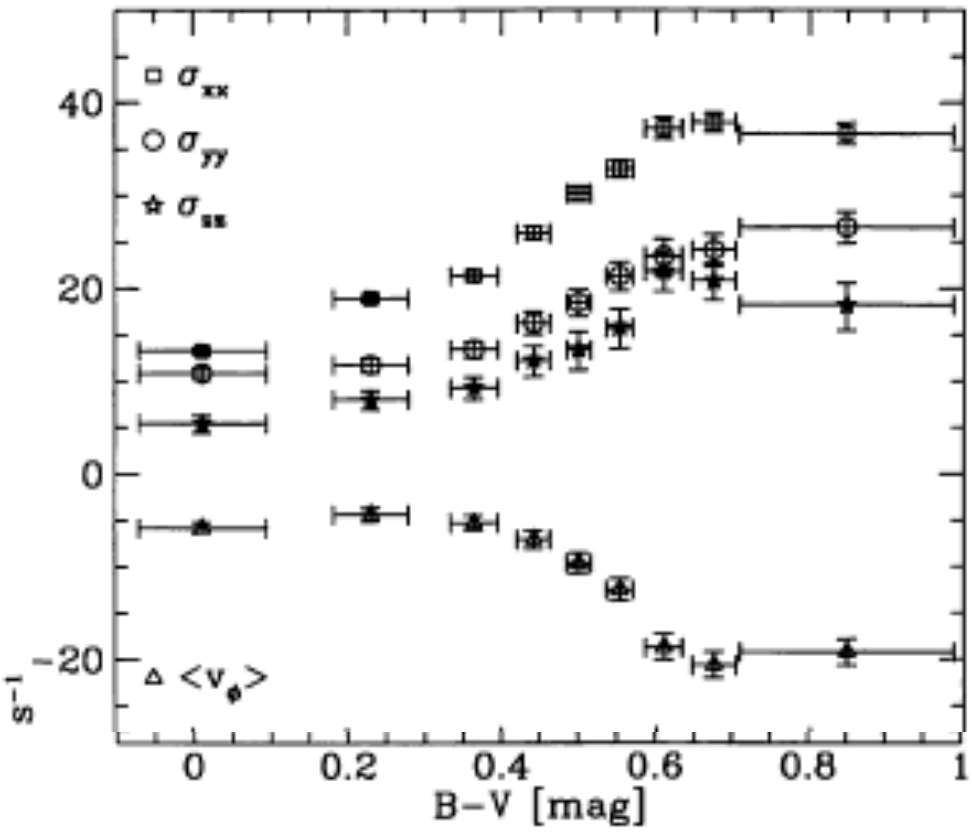

Figure 5. Velocity dispersions for stars in different colour bins. The top panel shows the mean rotation velocity (negative values imply lagging with respect to the LSR) and the three main velocity dispersions. In the three bottom panels $\sigma'_{ij} = \mathrm{sign}(\sigma^2_{ij})\,|\sigma^2_{ij}|^{1/2}$ is plotted for the mixed components of the tensor σ^2_{ij}.

we can measure κ/Ω, what about ν/Ω?

$$4\pi G\rho = \frac{1}{R}\frac{\partial}{\partial R}\left(R\frac{\partial \Phi}{\partial R}\right) + \frac{\partial^2 \Phi}{\partial z^2}$$
$$\simeq \frac{1}{R}\frac{\mathrm{d}v_\mathrm{c}^2}{\mathrm{d}R} + \nu^2, \quad \sim \nu^2$$

- *measure ν —> measure local matter density*
- *and since we are embedded in the disk…*
- *how do we go about this task?*
- *ratio of σ_z/σ_ϕ ?*

Table 1.1 Inventory of the solar neighborhood

component	volume density ($\mathcal{M}_\odot\,\mathrm{pc}^{-3}$)	surface density ($\mathcal{M}_\odot\,\mathrm{pc}^{-2}$)	luminosity density ($L_\odot\,\mathrm{pc}^{-3}$)	surface brightness ($L_\odot\,\mathrm{pc}^{-2}$)
visible stars	0.033	29	0.05	29
stellar remnants	0.006	5	0	0
brown dwarfs	0.002	2	0	0
ISM	0.050	13	0	0
total	0.09 ± 0.01	49 ± 6	0.05	29
dynamical	0.10 ± 0.01	74 ± 6	–	–

NOTES: Volume and luminosity densities are measured in the Galactic midplane and surface density is the total within ± 1.1 kpc of the plane. Luminosity density and surface brightness are given in the R band. Dynamical estimates are from §4.9.3. Most other entries are taken from Flynn et al. (2006).

Break-down of the epicycle approximation:

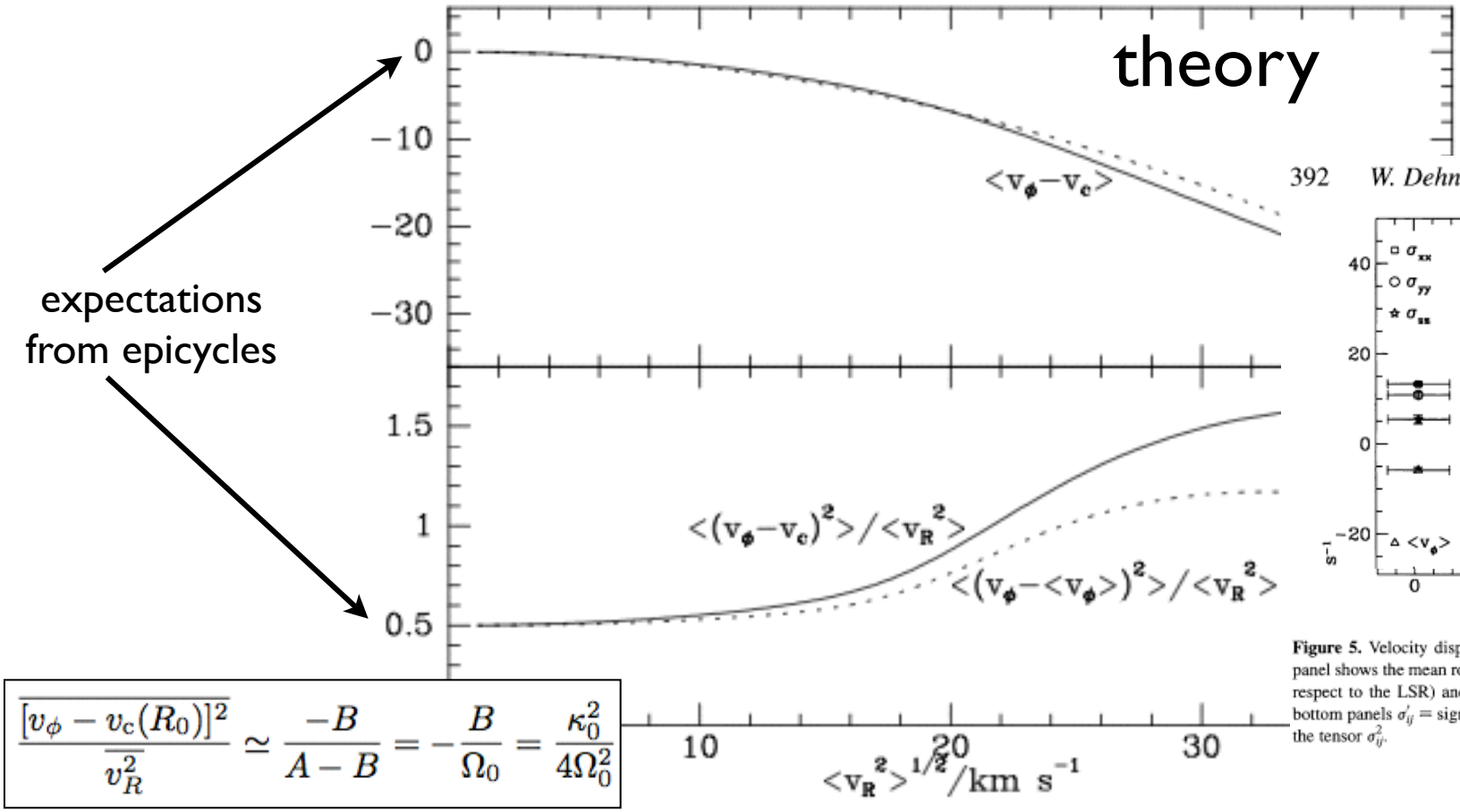

$$\frac{\overline{[v_\phi - v_c(R_0)]^2}}{\overline{v_R^2}} \simeq \frac{-B}{A-B} = -\frac{B}{\Omega_0} = \frac{\kappa_0^2}{4\Omega_0^2}$$

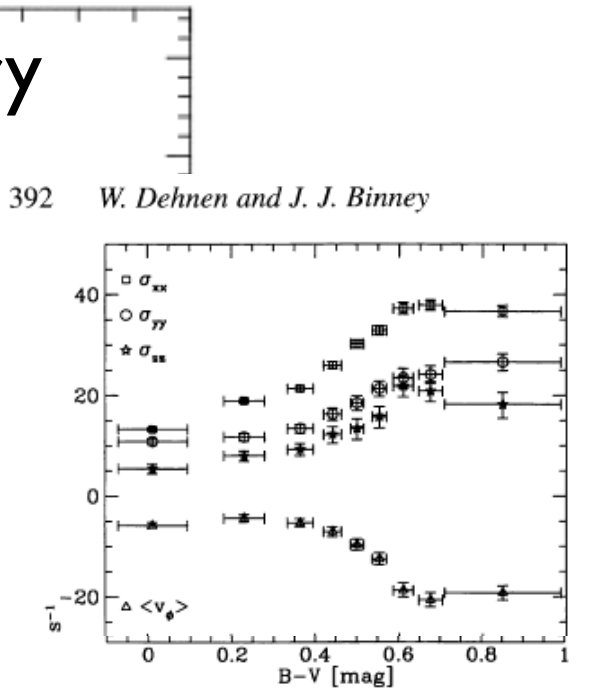

Figure 5. Velocity dispersions for stars in different colour bins. The tc
panel shows the mean rotation velocity (negative values imply lagging wit
respect to the LSR) and the three main velocity dispersions. In the thre
bottom panels $\sigma'_{ij} = \mathrm{sign}(\sigma^2_{ij})\,|\sigma^2_{ij}|^{1/2}$ is plotted for the mixed components
the tensor σ^2_{ij}.

Figure 4.16 Upper panel: the mean value of $\widetilde{v}_\phi$ as a function of $\overline{v_R^2}^{1/2}$ for azimuthal velocity distributions like those plotted in Figure 4.15. The dashed line shows a parabolic fit to the curve. Lower panel: for the same distributions the ratios $\overline{\widetilde{v}_\phi^2}/\overline{v_R^2}$ (full) and $\overline{(v_\phi - \overline{v}_\phi)^2}/\overline{v_R^2}$ (dashed).